

# SuperTIGER Ultra-Heavy Galactic Cosmic Ray Atmospheric Propagation Corrections and Validation

Nicole E. Osborn,<sup>a,\*</sup> Brian F. Rauch<sup>†,a</sup> and Wolfgang V. Zober<sup>a</sup> for the  
SuperTIGER Collaboration

<sup>a</sup>*Department of Physics and McDonnell Center for the Space Sciences, Washington University,  
St. Louis, MO 63130 USA*

*E-mail:* [n.osborn@wustl.edu](mailto:n.osborn@wustl.edu), [brauch@physics.wustl.edu](mailto:brauch@physics.wustl.edu), [wzober@wustl.edu](mailto:wzober@wustl.edu)

The SuperTIGER (Super Trans-Iron Galactic Element Recorder) balloon-borne ultra-heavy Galactic cosmic-ray (UHGCR) detector had successful Antarctic flights in 2012 (55 days) and 2019 (32 days). Stratospheric float altitudes varied between  $\sim 120,000 - 130,000$  ft, and measurements must be corrected for propagation through the residual  $\sim 0.5\%$  atmosphere using an approach developed for the preceding TIGER instrument. Changes due to nuclear interactions are determined iteratively starting from assumed top of the atmosphere (TOA) elemental abundances from which instrument abundances are found by solving networks of equations for all elements with partial and total charge-changing cross sections stepping through fine slabs of material and adjusting the TOA abundances after each run until the predicted instrument abundances match the flight measurements. Differential elemental atmospheric energy losses are corrected for using Geant4 simulations to find TOA minimum energies corresponding to the acrylic Cherenkov detector threshold ( $\sim 350$  MeV/nuc) and scaling TOA abundances corrected for nuclear interactions with the fraction of the integral energy spectrum for its TOA minimum energy, using the iron spectrum for the UHGCRs.

38th International Cosmic Ray Conference (ICRC2023)  
26 July - 3 August, 2023  
Nagoya, Japan



\*Speaker

<sup>†</sup>SuperTIGER supported by NASA under grant numbers NNX09AC17G, NNX14AB25G, NNX15AC23G, and 80NSSC20K0405 and the Peggy and Steve Fossett Foundation

## 1. Introduction

The best single element resolution measurements of the ultra-heavy Galactic cosmic rays (UHGCRs),  ${}_{30}\text{Zn}$  and higher charge elements, to-date have been made by the balloon-borne Super Trans-Iron Galactic Recorder (SuperTIGER) instrument [7, 8, 13, 14]. SuperTIGER is over four times the size of the predecessor TIGER instrument [5, 10, 11]. One advantage of balloon instruments is the larger geometric acceptances that can be flown than by space missions, but balloon-altitude measurements must be corrected for propagation through the residual atmosphere above the balloon. These corrections include those for nuclear interactions and energy losses in the instrument and atmosphere to derive top of the atmosphere (TOA) elemental abundances. SuperTIGER is nearly as large an UHGCR detector as can be flown on existing stratospheric balloons, and there is tension between detector size and weight versus higher altitude and reduced atmospheric burden.

The UHGCRs provide insight into the origins of the Galactic cosmic rays (GCRs), how they are accelerated, and the nucleosynthetic sources of the heavy elements. In Fig. 1 the relative abundances of elements from  ${}^1_1\text{H}$  to  ${}_{56}\text{Ba}$  for GCRs with energies of 2 GeV/nucleon are compared with the Solar System (SS) abundances [6] normalized to  ${}_{14}\text{Si}$ . These two samples of Galactic matter are nominally consistent, with most of the differences accounted for through cosmic ray spallation between the source and detection and by acceleration efficiencies. In the GCRs we see that  ${}_{26}\text{Fe}$  is  $\sim 5 \times 10^3$  times less abundant than  ${}^1_1\text{H}$ , the UHGCRs from  ${}_{30}\text{Zn}$  to  ${}_{40}\text{Zr}$  are  $\sim 10^5$  times less abundant than  ${}_{26}\text{Fe}$ , and the heavier UHGCRs are even more scarce still.

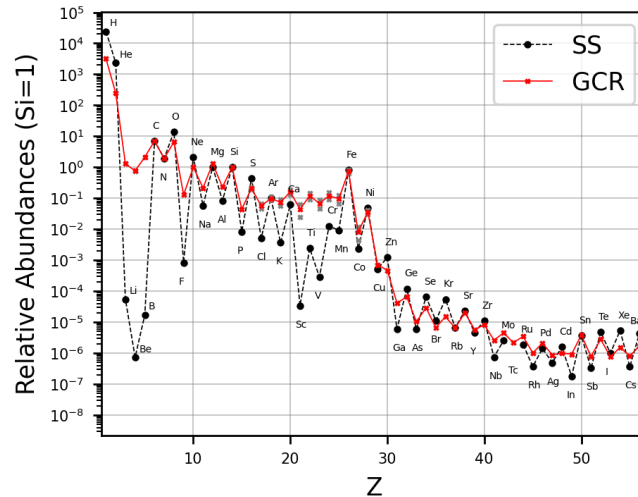


**Figure 1:** Solar System (SS) [6] and Galactic cosmic-ray (GCR) relative abundances at 2 GeV/nuc. The solid red line depicts average GCR data, sourced for  $1 \leq Z \leq 2$  from [12],  $Z=3$  from [1],  $4 \leq Z \leq 28$  from [3], and  $16 \leq Z \leq 56$  from [13] normalized to  ${}_{14}\text{Si}$ . The dashed black line depicts overlapping measurements from [3] and [13].

## 2. SuperTIGER

### 2.1 Instruments

SuperTIGER is a supersized ( $\sim 4\times$ ) version of the predecessor TIGER instrument. TIGER was a 1.16 m square 0.57 m tall stack of four compact wavelength-shifter readout scintillator detectors sandwiching scintillating optical fiber hodoscopes above and below silica aerogel and acrylic Cherenkov light collection box detectors. One of two SuperTIGER modules is shown in Fig. 2a and in an expanded view in Fig. 2b. SuperTIGER differs from TIGER in having only one scintillator at the top of the stack above the Cherenkov detectors to reduce the material in the GCR beam.

### 2.2 Flights

SuperTIGER had two successful Antarctic flights: SuperTIGER 2012 from December 8, 2012 - February 1, 2013 for 55 days with  $5.38 \times 10^6$   $^{26}\text{Fe}$  shown in Fig. 2c, and SuperTIGER 2019 from December 15, 2019 - January 17 2020 for 32 days with  $1.3 \times 10^6$   $^{26}\text{Fe}$  shown in Fig. 2d, where the UHGCR statistics scale with  $^{26}\text{Fe}$ . The first TIGER and SuperTIGER flights set duration records for zero-pressure heavy-lift stratospheric balloons, with the SuperTIGER record still standing.

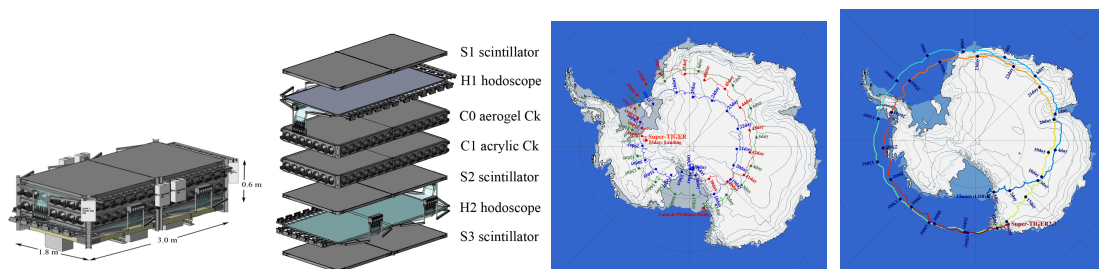


**Figure 2(a):** SuperTIGER module.

**Figure 2(b):** Expanded SuperTIGER module.

**Figure 2(c):** SuperTIGER 2012 flight.

**Figure 2(d):** SuperTIGER 2019 flight.

## 3. Atmospheric Propagation Corrections

To compare GCR abundances measured in the instrument with measurements in space it is necessary to first correct the abundances for the nuclear interactions and energy losses as particles travel down through the atmosphere and within the instrument. Corrections are first made for the propagation in the instrument, and the material above the first charge detector (top scintillator) must be handled differently from that in the active region where interacting particles can be identified. The material at the top of the instrument is included in the atmospheric corrections that account for both loss and gain of each element through nuclear interactions, while within the active area of the detector only corrections for loss are made since interaction cuts have been applied. The inactive material above the top scintillator detectors was modeled with an equivalent depth of atmosphere in the propagation corrections, with  $1.31 \text{ g/cm}^2$  for TIGER and  $0.1 \text{ g/cm}^2$  for SuperTIGER based on the material above the top scintillator given in Table 2. Nuclear interaction probabilities and the rate of energy loss both increase for nuclei with higher  $Z$ , where energy loss increases as  $Z^2$  and interactions increase with nuclear cross sectional area  $\sim A^{2/3}$ , where  $A \propto Z$ .

### 3.1 Cross Sections

TIGER and SuperTIGER cannot discriminate between isotopes, so the atmospheric and instrument propagation corrections use total and partial charge-changing cross sections. The total charge-changing cross sections are used to correct for nuclear interaction losses for each projectile element in the propagation. Partial charge-changing cross sections correct for nuclear interaction gains. Each partial cross section for a given projectile is calculated at a  $\Delta Z$ , the change in charge a projectile nuclei experiences. The sum of all partial charge-changing cross sections across all  $\Delta Z$  for a given projectile should equal the total charge-changing cross section for that projectile.

The total charge-changing cross sections are given by

$$\sigma_{tot}(P, T) = \pi [R_P + R_T - (3.20 \pm 0.05)]^2, \quad (1)$$

where  $P$  and  $T$  refer to the projectile and target nuclei, and  $R_P$  and  $R_T$  are their respective nuclear radii. The nuclear radii have a hard sphere fitting parameter,  $S$ , that relates to the electron radii by  $R_n = SR_e$ . This parameter is  $S=1.277 \pm 0.006$  with a  $\chi^2 = 5.59$  [9], which was used in the calculation of  $R_P$  and  $R_T$ . The total charge-changing cross sections are given in Fig. 3a for the materials used in the atmospheric propagation and instrument correction, showing the increase in the cross sections is less than linear in  $Z$ .

The partial charge-changing cross sections are given by

$$\sigma_{\Delta Z}(A_P, A_T, K, \Delta Z) = p_1(A_P^{1/3} + A_T^{1/3} - p_2)(1 + p_3/K)|\Delta Z|^{-p_4[1+A_P^{1/3}/p_5+A_T^{1/3}/p_6+p_7/K]}, \quad (2)$$

where  $A_P$  and  $A_T$  are the atomic masses of the projectile and target nuclei,  $\Delta Z$  is the change in charge of the projectile,  $K$  is the total kinetic energy of the projectile, and the parameters are given in Table 1. For this analysis a value of  $K = 2A$  GeV was selected as representative for the TIGER GCRs and  $K = 3.1A$  GeV was chosen for the SuperTIGER GCRs. The total charge-changing cross sections are shown in Fig. 3a for projectile targets in the atmosphere and material in the detector.

To ensure the total charge-changing cross section for an element equals the sum of the partial charge-changing cross sections, a weight factor was introduced to scale the partial charge-changing cross sections. The weight factors are introduced after calculating the total charge-changing cross section at each element using Equation 1 and the sum over  $\Delta Z$  for each partial charge-changing cross section from Equation 2. A scaling value is varied until the sum over  $\Delta Z$  of the partial charge-changing cross sections are equal to the total cross section at a given  $Z$ . The charge dependence of the weight factor given in Fig. 4 is non-linear in charge, especially at low  $Z$ . These corrected factors produce total and partial charge-changing cross sections for the projectile elements from  ${}_{27}\text{Ni}$  to  ${}_{40}\text{Zr}$  for the atmospheric gas targets of  ${}_{7}\text{N}$  and  ${}_{8}\text{O}$ , as shown in Fig. 3b and Fig. 3c, respectively.

parameter	value
$p_1$	$21.2 \pm 0.5$ mb
$p_2$	$1.08 \pm 0.15$
$p_3$	$(0.485 \pm 0.014)A$ GeV
$p_4$	$0.094 \pm 0.013$
$p_5$	$1.11 \pm 0.02$
$p_6$	$10.8 \pm 1.6$
$p_7$	$(0.85 \pm 0.03)A$ GeV
$\chi^2_{\nu}$	2.84
$N$	1741

**Table 1:** Partial charge-changing cross section parameters taken from Table VIII in the paper [9].

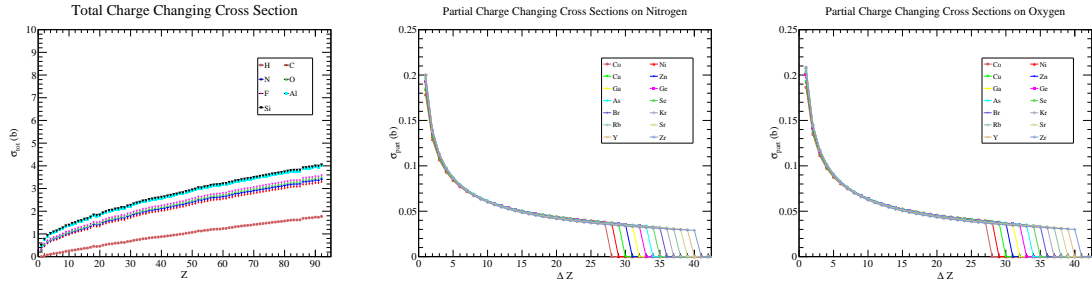


**Figure 3(a):** Total charge-changing cross sections of projectile nuclei on target nuclei  $^1\text{H}$ ,  $^6\text{C}$ ,  $^7\text{N}$ ,  $^8\text{O}$ ,  $^9\text{F}$ ,  $^{13}\text{Al}$ , and  $^{14}\text{Si}$ . **Figure 3(b):** Partial charge-changing cross sections on  $^{14}\text{N}$  for targets  $^{27}\text{Co}$  to  $^{40}\text{Zr}$ . **Figure 3(c):** Partial charge-changing cross sections on  $^{16}\text{O}$  for targets  $Z = 27\text{Co}$  to  $^{40}\text{Zr}$ .

### 3.2 Instrument and Energy Correction

The measured abundances are corrected to the top detector for interaction losses in the active instrument area in TIGER [5, 10, 11] and SuperTIGER [7, 8, 13]. Corrections for the inactive detector material above the middle of the top scintillator radiators in TIGER and SuperTIGER are listed in Table 2 were folded into the corrections for interactions in the atmosphere. The top insulation for SuperTIGER is melamine ( $\text{C}_3\text{H}_6\text{N}_6$ ) foam, but foam is polymerized melamine-sodium bisulfite ( $\text{C}_9\text{H}_6\text{Na}_6\text{S}_6\text{O}_{18}$ ), which is presumed to lose H in polymer linkages, at least two per molecule to form a strand and more for cross linkages. To date this material has been approximated as acrylic.

detector material	chemical formula	TIGER top	TIGER active	ST top	ST active
PET	$\text{C}_{10}\text{H}_8\text{O}_4$	0.102	0	0.025	0.062
PMMA	$\text{C}_5\text{H}_8\text{O}_2$	0	0.938	0.040	1.499
aluminum	Al	0.148	0.07	0.033	0.372
PS	$\text{C}_8\text{H}_8$	0.342	1.920	0	0.388
PVT	$\text{C}_9\text{H}_{10}$	0.412	1.442	0.523	1.057
silica	$\text{SiO}_2$	0	0.586	0	0.614

**Table 2:** TIGER and SuperTIGER instrument materials above the middle of the first scintillator detector (top) and in average in the active area (active) in  $\text{g}/\text{cm}^2$ : polyethylene terephthalate (PET) - Mylar, polymethyl methacrylate (PMMA) - acrylic, aluminum (Al), polystyrene (PS), polyvinyltoluene (PVT), silica  $\text{SiO}_2$ .

A correction for energy losses is made by calculating the minimum energy at the top of the atmosphere required to be above threshold in the acrylic Cherenkov detector based on the average energy losses in detector materials and the atmosphere. The top of the atmosphere abundances corrected for interactions in the atmosphere are then renormalized compared to  $^{26}\text{Fe}$  based on evaluating the normalized integral spectrum of each element derived from differential spectra [4]

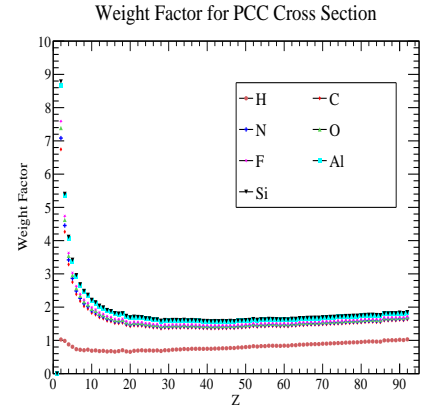


**Figure 4:** Partial charge-changing cross section scaling for each element.

First Step	Last Step	Difference
115600.8876	115168.5385	0.3747 %

**Table 3:** The total charge abundance at the first step of the iteration compared to the final step.

for elements below  ${}_{26}\text{Ni}$  and scaled  ${}_{26}\text{Fe}$  spectra for UHGCRs.

### 3.3 Propagation

In the atmosphere and instrument materials, the correction process tracks the charge-changing interactions that will add to or reduce the flux of each element in passing through the material above the active instrument. The total and partial charge-changing cross sections are used to correct SuperTIGER measured abundances to TOA abundances. Initial TOA abundances in the model are assumed using satellite GCR measurements from HEAO-3-C2, HEAO-3-C3, and Ariel [2, 3]. Initial TOA abundances are iterated down through slabs of material for  $n_{step}=1000$  steps. The abundance of a projectile in a step  $i+1$  of atmosphere is calculated using the abundance at step  $i$  and adjusting for the losses and gains due to nuclear interactions as  $J_{i+1}(P) = J_i(P) - L_i(P) + G_i(P)$ . The loss term is given by

$$L_i(P) = J_i(P) 10^{-24} \frac{N_{atm}}{n_{step}} N_A (\sigma_{tot,N}(P, N) r_N + \sigma_{tot,O}(P, N) r_O), \quad (3)$$

where  $N_{atm}$  is the surface mole density of the atmosphere,  $N_A$  is Avogadro's Number,  $\sigma_{tot}(P)$  is the total charge-changing cross section for a projectile  $P$  on the target with  $r_N$  and  $r_O$  being the number fractions of nitrogen and oxygen in the atmosphere, respectively. The gain term, which produces two daughter nuclei is given by

$$G_i(P) = \sum_{\Delta Z = Z(P') - Z(P) > 0} \left[ J_i(P') 10^{-24} \frac{N_{atm}}{n_{step}} N_A (\sigma_{\Delta Z, N} r_N + \sigma_{\Delta Z, O} r_O) \right], \quad (4)$$

where the sum is over all  $\Delta Z$  where the charge of a projectile  $P'$  is greater than the charge of a projectile  $P$ .  $\sigma_{\Delta Z}$  is the partial charge-changing cross section of a projectile  $P'$  with a given  $\Delta Z$  from interacting with a target nuclei  ${}_{7}\text{N}$  or  ${}_{8}\text{O}$ . At the final step in the propagation, the abundance at each element is compared to the measured abundance from the active area in the detector. The initial TOA is then adjusted and the propagation is performed again, until all initial TOA abundances are propagated down the atmosphere to equal the instrument (TOI) abundance.

To confirm that charge is conserved in the propagation the total is calculated at each step by multiplying the charge by the absolute abundance of each element to confirm that during the propagation the charge is conserved. The TOA charge compared with the charge after propagation changes by less than 0.4%, see Table 3.

## 4. Results and Discussions

Atmospheric nuclear interaction corrections using total and partial charge-changing cross sections produce TOA abundances consistent with SuperTIGER raw abundances. Introducing a

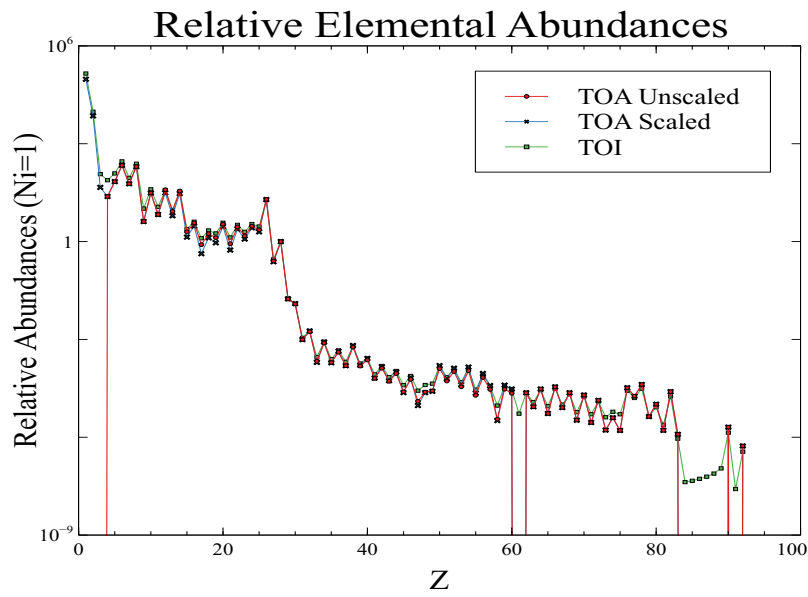


**Figure 5(a):** TOA and TOI relative abundances after scaling the partial charge-changing cross sections (blue, purple) compared with abundances without scaling the partial charge-changing cross sections (red, purple).

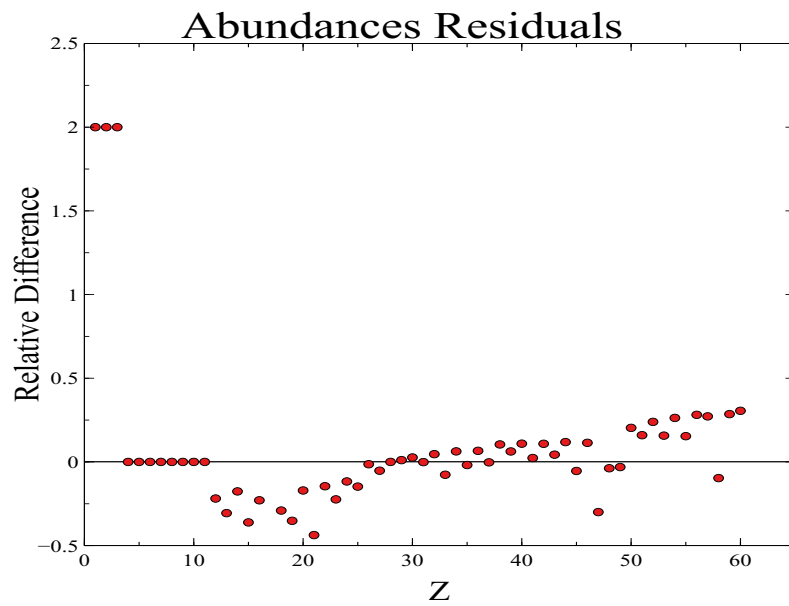


**Figure 5(b):** Residuals between the abundances from the scaled and unscaled charge-changing cross sections.

weight factor for the partial charge-changing cross sections affects the propagation model leading to different final abundances compared to the unscaled partial charge-changing cross sections.

The TOA relative abundances are shown with both the scaled and unscaled partial charge-changing cross sections in Fig. 5a, along with the corresponding TOI abundance. The most significant abundance changes from scaling were in  $Z > 10\text{Ne}$ . The residual plot comparing TOA scaled and unscaled is seen in Fig. 5b.

The next step in this analysis is to fully implement a Monte Carlo method to estimate systematic uncertainties by simultaneously and randomly varying atmospheric propagation total and partial charge-changing cross sections over Gaussian distributions with widths determined by uncertainties. Further down the line the goal is to use simulations for a more advanced model of nuclear interactions in the atmosphere.

## 5. Acknowledgements

The material contained in this document is based upon work supported by a National Aeronautics and Space Administration (NASA) grant or cooperative agreement. Any opinions, findings, conclusions, or recommendations expressed in this material are those of the author and do not necessarily reflect the views of NASA.

## 6. References

- [1] M. Aguilar et al. Isotopic Composition of Light Nuclei in Cosmic Rays: Results from AMS-01. *The Astrophysical Journal*, 736(2):105, Aug. 2011.
- [2] W. R. Binns, T. L. Garrard, P. S. Gibner, M. H. Israel, M. P. Kertzman, J. Klarmann, B. J. Newport, E. C. Stone, and C. J. Waddington. Abundances of Ultraheavy Elements in the Cosmic Radiation: Results from HEAO 3. , 346:997, Nov. 1989.
- [3] J. J. Engelmann, P. Ferrando, A. Soutoul, P. Goret, E. Juliusson, L. Koch-Miramond, N. Lund, P. Masse, B. Peters, N. Petrou, and I. L. Rasmussen. Charge composition and energy spectra of cosmic-ray nuclei for elements from Be to Ni - Results from HEAO-3-C2. , 233:96–111, July 1990.
- [4] J. S. George et al. Elemental Composition and Energy Spectra of Galactic Cosmic Rays During Solar Cycle 23. *The Astrophysical Journal*, 698(2), 2009.
- [5] J. T. Link. *Measurements of Ultra-Heavy Galactic Cosmic Rays with the TIGER Instrument*. PhD thesis, Washington University in St. Louis, 2003.
- [6] K. Lodders. Solar System Abundances and Condensation Temperatures of the Elements. *The Astrophysical Journal*, 519:1220–1247, 2003.
- [7] R. P. Murphy. *Identifying the Origin of Galactic Cosmic Rays with the SuperTIGER Instrument*. PhD thesis, Washington University in St. Louis, 2015.
- [8] R. P. Murphy et al. Galactic Cosmic Rays Origins and OB Associations: Evidence from SuperTIGER Observations of Elements  $_{26}\text{Fe}$  through  $_{40}\text{Zr}$ . *The Astrophysical Journal*, 831(2):148, 2016.
- [9] B. S. Nilsen et al. Fragmentation Cross Sections of Relativistic  $^{84}_{36}\text{Kr}$  and  $^{109}_{47}\text{Ag}$  Nuclei in Targets From Hydrogen to Lead. *Physical Review C*, 52(6):3277–3290, 1995.
- [10] B. F. Rauch. *Measurement of the Relative Abundances of the Ultra-Heavy Galactic Cosmic Rays ( $30 \leq Z \leq 40$ ) with the Trans-Iron Galactic Element Recorder (TIGER) Instrument*. PhD thesis, Washington University in St. Louis, 2008.
- [11] B. F. Rauch, J. T. Link, K. Lodders, M. H. Israel, L. M. Barbier, W. R. Binns, E. R. Christian, J. R. Cummings, G. A. de Nolfo, S. Geier, R. A. Mewaldt, J. W. Mitchell, S. M. Schindler, L. M. Scott, E. C. Stone, R. E. Streitmatter, C. J. Waddington, and M. E. Wiedenbeck. Cosmic Ray Origin in OB Associations and Preferential Acceleration of Refractory Elements: Evidence from Abundances of Elements  $_{26}\text{Fe}$  through  $_{34}\text{Se}$ . *The Astrophysical Journal*, 697(2):2083–2088, 2009.
- [12] T. Sanuki et al. Precise Measurement of Cosmic-Ray Proton and Helium Spectra with the BESS Spectrometer. *The Astrophysical Journal*, 545(2):1135–1142, 2000.
- [13] N. E. Walsh. *SuperTIGER Elemental Abundances for the Charge Range  $41 \leq Z \leq 56$* . PhD thesis, Washington University in St. Louis, 2020.
- [14] N. E. Walsh et al. SuperTIGER Abundances of Galactic Cosmic Rays for the Atomic Number ( $Z$ ) Interval 30 to 56. In *Proceedings of 37th International Cosmic Ray Conference — PoS(ICRC2021)*, volume 395, page 118, 2021.

**Full Author List: SuperTIGER Collaboration**

Q. Abarr<sup>1</sup>, Y. Akaike<sup>2</sup>, W. R. Binns<sup>1</sup>, T. J. Brandt<sup>2</sup>, D. L. Braun<sup>1</sup>, J. H. Buckley<sup>1</sup>, N. W. Cannady<sup>3,2,4</sup>, R. M. Crabill<sup>5</sup>, G. A. de Nolfo<sup>6</sup>, P. F. Dowkontt<sup>1</sup>, S. P. Fitzsimmons<sup>2</sup>, P. Ghosh<sup>7,2,4</sup>, T. Hams<sup>8</sup>, M. H. Israel<sup>1</sup>, J. F. Krizmanic<sup>2</sup>, W. Labrador<sup>1</sup>, A. W. Labrador<sup>5</sup>, L. Lisalda<sup>1</sup>, R. A. Mewaldt<sup>5</sup>, J. G. Mitchell<sup>6</sup>, J. W. Mitchell<sup>2</sup>, R. P. Murphy<sup>1</sup>, S. Nutter<sup>9</sup>, M. A. Olevitch<sup>1</sup>, N. E. Osborn<sup>1</sup>, B. F. Rauch<sup>1</sup>, K. Sakai<sup>3,2,4</sup>, M. Sasaki<sup>10,2,4</sup>, F. S. Sebastian<sup>2</sup>, G. E. Simburger<sup>1</sup>, E. C. Stone<sup>5</sup>, T. Tatoli<sup>3,2,4</sup>, N. E. Walsh<sup>1</sup>, J. E. Ward<sup>1</sup>, A. T. West<sup>1</sup>, M. E. Wiedenbeck<sup>11</sup>, W. V. Zober<sup>1</sup>,

<sup>1</sup>Department of Physics and McDonnell Center for the Space Sciences, Washington University in St. Louis, <sup>2</sup>NASA Goddard Space Flight Center, Astrophysics Science Division, <sup>3</sup>University of Maryland, Baltimore County, <sup>4</sup>Center for Research and Exploration in Space Sciences and Technology II, <sup>5</sup>California Institute of Technology, <sup>6</sup>NASA Goddard Space Flight Center, Heliophysics Science Division, <sup>7</sup>Catholic University of America, <sup>8</sup>NASA, <sup>9</sup>Northern Kentucky University, <sup>10</sup>University of Maryland, College Park, <sup>11</sup>NASA Jet Propulsion Laboratory,

POS (ICRC2023) 173